ATP citrate lyase inhibition can suppress tumor cell growth

Georgia Hatzivassiliou,[1] Fangping Zhao,[1] Daniel E. Bauer,[1] Charalambos Andreadis,[2] Anthony N. Shaw,[3] Dashyant Dhanak,[4] Sunil R. Hingorani,[1,2] David A. Tuveson,[1,2] and Craig B. Thompson[1,*]

[1]Department of Cancer Biology, Abramson Family Cancer Research Institute, University of Pennsylvania, Philadelphia, Pennsylvania 19104
[2]Department of Medicine, Abramson Cancer Center, University of Pennsylvania, Philadelphia, Pennsylvania 19104
[3]Department of Medicinal Chemistry, Metabolic and Viral Diseases Center of Excellence for Drug Discovery, GlaxoSmith-Kline, Collegeville, Pennsylvania 19426
[4]Department of Medicinal Chemistry, Musculoskeletal, Microbial and Proliferative Diseases Center of Excellence for Drug Discovery, GlaxoSmith-Kline, Collegeville, Pennsylvania 19426
*Correspondence: craig@mail.med.upenn.edu

Summary

Many tumors display a high rate of glucose utilization, as evidenced by 18-F-2-deoxyglucose PET imaging. One potential advantage of catabolizing glucose through glycolysis at a rate that exceeds bioenergetic need is that the growing cell can redirect the excess glycolytic end product pyruvate toward lipid synthesis. Such de novo lipid synthesis is necessary for membrane production and lipid-based posttranslational modification of proteins. A key enzyme linking glucose metabolism to lipid synthesis is ATP citrate lyase (ACL), which catalyzes the conversion of citrate to cytosolic acetyl-CoA. ACL inhibition by RNAi or the chemical inhibitor SB-204990 limits in vitro proliferation and survival of tumor cells displaying aerobic glycolysis. The same treatments also reduce in vivo tumor growth and induce differentiation.

Introduction

Many human cancers display a high rate of aerobic glycolysis (Warburg, 1956), a phenomenon that is exploited in 18-F-2-deoxyglucose positron emission tomography (FDG-PET) imaging for the detection of primary and metastatic tumors (Gambhir, 2002). Upregulation of glycolytic metabolism occurs downstream of multiple oncogenic pathways (Dang and Semenza, 1999; Elstrom et al., 2004) and has been shown to correlate with increased tumor aggressiveness and poor patient prognosis in several tumor types (Detterbeck et al., 2004). These observations suggest that the glycolytic phenotype plays a role in tumor progression by contributing to tumor growth or survival.

High levels of glycolysis not only provide ATP for the tumor cells' high bioenergetic demands but may also provide precursors and reducing equivalents for the synthesis of macromolecules, such as nucleotides, proteins, and lipids. In most tissues, fatty acid synthesis occurs at low rates since lipids are acquired via the circulation to support the needs of vegetative nonproliferating cells. In contrast, de novo fatty acid synthesis occurs at very high rates in tumor tissues (Kuhajda, 2000), as first demonstrated more than half a century ago (Medes et al., 1953). ^{14}C glucose studies have shown that in tumor cells almost all fatty acids are derived from de novo synthesis despite an abundant supply of extracellular lipids (Ookhtens et al., 1984; Sabine et al., 1967). The high rate of de novo fatty acid synthesis in rapidly proliferating cells fuels membrane biogenesis (Jackowski et al., 2000; Zambell et al., 2003). It is thus possible that an increase in the uptake and metabolism of glucose contributes to enhanced tumor cell proliferation by promoting de novo fatty acid synthesis.

The pathway for glucose-dependent de novo lipogenesis is illustrated in Figure 1. In cells that have undergone a glycolytic conversion, i.e., have shifted from an oxidative to a glycolytic mode of metabolism under aerobic conditions, much of the bioenergetic supply is provided through glycolytic ATP production (Nakashima et al., 1984), and glycolytically derived pyruvate enters a truncated TCA cycle (Baggetto, 1992; Crabtree, 1929) where citrate is preferentially exported to the cytosol via the tricarboxylate transporter (Kaplan et al., 1993). Once in the cytosol, citrate is cleaved by ATP citrate lyase (ACL) to produce cytosolic acetyl-CoA and regenerate oxaloacetate (Figure 1) (Srere, 1959). Acetyl-CoA is the requisite building block for the endogenous synthesis of fatty acids, cholesterol, and isoprenoids as well as acetylation reactions that modify proteins. To

SIGNIFICANCE

A common feature of human cancer is the conversion to a glucose-dependent form of metabolism. When a tumor cell's glucose metabolism exceeds its bioenergetic needs, the excess metabolites can be secreted as lactate or diverted toward the intracellular synthesis of lipids. Lipid synthesis is required by a growing cell to synthesize membranes and lipid-modified signaling molecules. As the regulator of the key step that can convert high glycolytic flux into increased lipid synthesis, ATP citrate lyase (ACL) is identified as a potential molecular target for cancer therapy. This report validates ACL as a therapeutic target and provides the rationale for the development of ACL inhibitors as antineoplastic agents against human tumors that have undergone a glycolytic conversion.

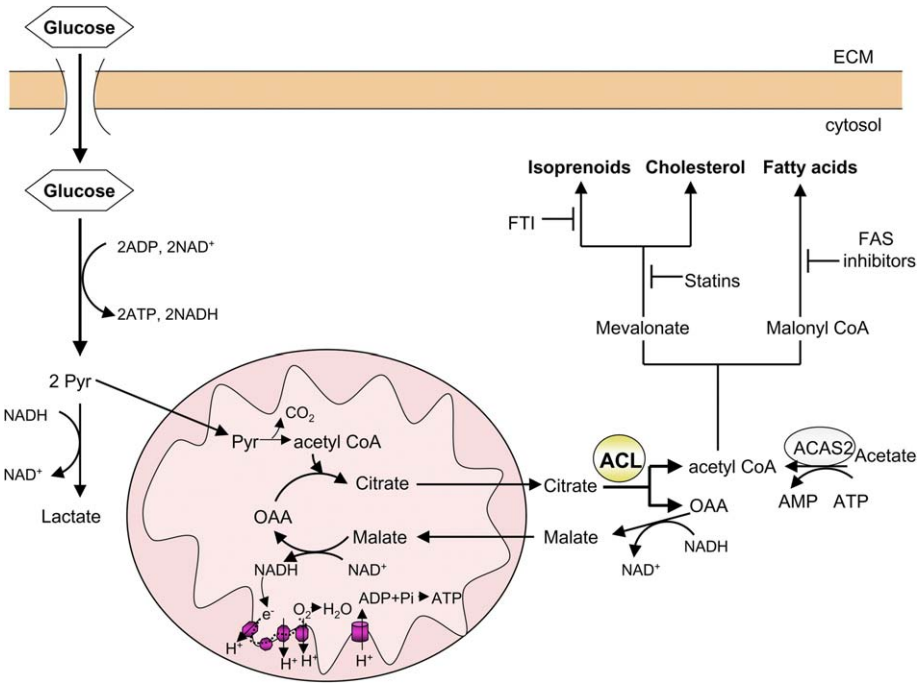

Figure 1. ATP citrate lyase regulates the flow of glucose carbons to cytosolic acetyl-CoA during glucose catabolism

Upon stimulation of aerobic glycolysis, increased glucose uptake and increased flux of glucose carbons into the mitochondria as pyruvate leads to an increase in the mitochondrial concentration of citrate. Mitochondrial citrate is transported down a concentration gradient to the cytosol. ATP citrate lyase (ACL) cleavage of cytosolic citrate generates acetyl-CoA and oxaloacetate. Acetyl-CoA is the precursor for the synthesis of fatty acids, cholesterol, and isoprenoids, while oxaloacetate is reduced to malate, using NADH as an electron donor. Malate returns to the mitochondrial matrix, where it is oxidized to regenerate oxaloacetate. The resulting NADH donates its electrons to the electron transport chain to maintain the inner membrane potential and oxidative phosphorylation. Under conditions of low cellular glucose uptake, an alternative pathway for the generation of cytosolic acetyl-CoA is through the activation of acetate by acetyl-CoA synthetase. ACL, ATP citrate lyase; ACAS2, acetyl-CoA synthetase; FAS, fatty acid synthesis; OAA, oxaloacetate; Pyr, pyruvate; FTI, farnesyl transferase inhibitors; ECM, extracellular matrix. (See text for details.)

complete this substrate cycle, ACL-generated oxaloacetate is reduced to malate, which can return to the mitochondria, recycling carbon and shuttling reducing equivalents into the mitochondria (Figure 1). The conversion of cytosolic oxaloacetate to malate is driven by the high cytosolic NADH/NAD+ ratio present in glycolytic cells (Bauer et al., 2004). Malate can enter the mitochondrial matrix and be converted there to oxaloacetate to complete the substrate cycle. The coupled conversion of NAD+ to NADH provides a continuing mechanism to preserve the mitochondrial membrane potential (MMP) and sustain a high mitochondrial NADH/NAD+ ratio that maintains the TCA cycle in a repressed state. Thus, ACL enzymatic activity is poised to affect both glucose-dependent lipogenesis and cellular bioenergetics.

ACL is a homotetrameric enzyme with widespread tissue expression, which exhibits coordinate transcriptional regulation with other enzymes in the lipogenic pathway. ACL levels increase in response to signals that communicate nutritional status, activate cellular glucose uptake and metabolism, and stimulate anabolic growth (Towle et al., 1997). Insulin transcriptionally induces and activates ACL through the PI3K/Akt pathway in insulin-responsive tissues and tissue-specific growth factors that activate the PI3K/Akt pathway appear to play a similar role in other tissues (Towle et al., 1997). Insulin and growth factor stimulation also lead to ACL phosphorylation by Akt (Berwick et al., 2002; Buzzai et al., 2005). Furthermore, high levels of glucose increase ACL levels synergistically with PI3K/Akt activation (Katz and Giffhorn, 1983). It thus becomes evident that signaling pathways that contribute to a glycolytic phenotype and play an important role in tumorigenesis can also lead to increased ACL levels and/or activity. These pathways may partly account for the fact that ACL activity was found to be significantly elevated in breast (Szutowicz et al., 1979) and bladder (Turyn et al., 2003) carcinomas versus normal breast and bladder tissue: 160-fold and 7-fold, respectively.

Based on ACL's potential role in the integration of glucose and lipid metabolism, we have assessed its potential as a therapeutic target for cancer. For this purpose, we used both genetic and pharmacological approaches to demonstrate that ACL inhibition results in the suppression of proliferation and the promotion of differentiation in glucose-dependent tumors. These data suggest that tumors that have undergone a metabolic conversion to aerobic glycolysis utilize the glucose-dependent production of cytosolic acetyl-CoA to fuel lipid synthesis. Thus, conversion to aerobic glycolysis appears to be capable of promoting tumor growth by both stimulating lipid synthesis and suppressing tumor cell differentiation. These properties may contribute to selection for conversion to aerobic glycolysis during tumor progression in vivo (the Warburg effect). ACL inhibitors appear to have the potential to suppress the growth of such advanced malignancies, a group that has otherwise proven highly resistant to existing therapeutic strategies.

Results

Knockdown of endogenous ACL levels by siRNA disturbs mitochondrial homeostasis and impairs the proliferation and viability of tumor cells

To assess the effects of ACL inhibition on tumor cells, RNA interference (RNAi) was used to reduce ACL levels in the human lung adenocarcinoma cell line A549. Transient transfection of A549 cells with the ACL siRNA oligonucleotide (siACL) led to a progressive decline in ACL protein levels compared to a luciferase siRNA (siLUC) control. The decline in ACL protein was modest at 24 hr post-siRNA treatment but became gradually more pronounced by 48 and 72 hr posttransfection (Fig-

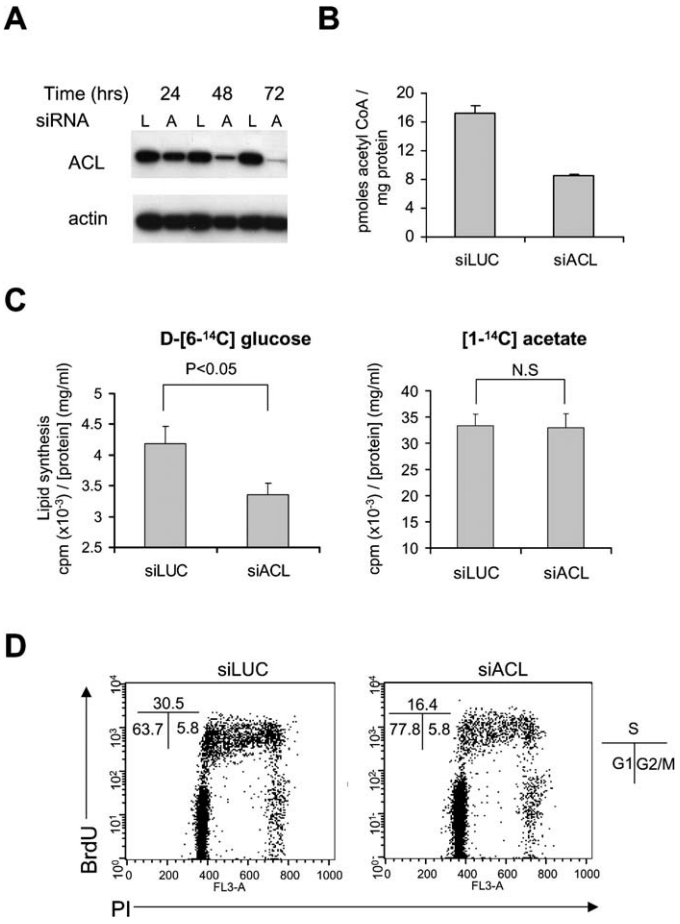

Figure 2. Effects of ACL knockdown by transient RNAi on lipid synthesis and cell cycle progression in a human lung adenocarcinoma line

A: siRNA oligonucleotides targeting luciferase ("L") or ACL ("A," corresponding to the ACL4 siRNA sequence) were transiently transfected into A549 cells, and protein extracts were analyzed for ACL expression at the indicated times posttransfection.

B: Levels of total cellular acetyl-CoA were compared in siLUC- versus siACL-treated cells 7 days posttransfection as described in the Experimental Procedures and were normalized to protein concentration. Data shown are the mean ± SEM of triplicate samples from a representative experiment.

C: Glucose-dependent (left panel) versus acetate-dependent (right panel) lipid synthesis was compared in siLUC- versus siACL-treated cells 48 hr posttransfection. Counts for each sample were normalized to protein concentration. Data shown are the mean ± SEM of triplicate samples from a representative experiment.

D: siLUC (left panel) or siACL (right panel)-treated cells were pulse labeled with 10 μM BrdU 72 hr posttransfection and analyzed for BrdU incorporation and DNA content (PI). The percentage of cells in the G1, S, and G2/M phases is indicated for representatives of triplicate samples.

ure 2A). To document the effects of ACL downregulation on acetyl-CoA synthesis, acetyl-CoA levels in siLUC- and siACL-treated cells were compared. Persistent repression of ACL synthesis resulted in a 50% reduction in total acetyl-CoA levels in the siACL-treated cells compared to controls (Figure 2B). As early as 48 hr posttransfection, a significant decline in D-[6-^{14}C] glucose-dependent lipid synthesis was observed in the siACL-treated cells (Figure 2C). Lipid synthesis through [1-^{14}C]acetate, which is converted to acetyl-CoA by acetyl-CoA synthetase (ACAS2) and not ACL (Figure 1) was unaffected (Figure 2C). By 72 hr, cell accumulation in the siACL-treated population was considerably slower than that of siLUC-treated cells. siACL-treated cells exhibited an increase in the percentage of cells in the G1 phase accompanied by a decrease in S phase cells, in comparison to control cells (Figure 2D). This resulted in a 30% decline in the cell number of ACL siRNA-treated cells compared to controls but no difference in cell viability (data not shown).

To observe the effects of prolonged ACL inhibition, cells were treated as described in Figure 2, with siLUC or two independent ACL siRNAs (siACL1 and siACL4) for 72 hr, and then replated at equal numbers and subjected to a second round of siRNA transfection. During this second transfection period, ACL protein remained at near undetectable levels (Figure 3A). Mitochondrial effects were consistently observed during these experiments. A time-dependent increase in MMP in ACL knockdown cells first became apparent 72 hr posttransfection (round 1) and was maintained for the duration of the second siRNA transfection round (Figure 3B). Cell proliferation was severely impaired, since the cell number of ACL knockdown cells remained stable, while control cells continued to proliferate (Figure 3C). Cell viability remained high, and a decrease in the viability of ACL knockdown cells was observed only at late time points (Figure 3D).

Stable knockdown of endogenous ACL levels by shRNA suppresses tumor growth in vivo and induces glandular differentiation in A549 lung adenocarcinoma cells

In order to study the effects of stable *ACL* gene knockdown on the in vivo tumorigenicity of A549 cells, we generated expression constructs containing ACL short hairpin RNAs (shRNAs) and established stable clones of A549 with shRNA-mediated suppression of ACL. Two independent constructs, pKD-ACL4 (HP 4) and pKD-ACL1 (HP 1), were used to generate stable cell lines with efficient ACL knockdown (Figure 4A). Two clones (HP 4-7 and HP 4-8) stably transfected with pKD-ACL4 and displaying significantly reduced ACL levels (Figure 4A) were analyzed in detail. In concordance with the observed reduction in ACL protein levels (Figure 4A), ACL activity in these clones decreased at least 10-fold (Figure 4B).

To determine their tumorigenicity in vivo, we injected vector control (V6) and ACL knockdown clones (HP 4-7 and HP 4-8) subcutaneously into nude mice and examined tumor formation and progression. Injections were done in such a manner that each mouse received a vector control inoculation in one flank and an ACL shRNA clone in the other, so that tumor comparisons would be controlled for each individual mouse. The growth of tumors was monitored weekly, and tumors were excised and weighed 60 days postinjection. The results demonstrate that ACL knockdown cells form significantly smaller tumors in vivo (Figure 4C). Western blotting of protein lysates from the excised tumors confirmed maintenance of the ACL knockdown phenotype by the tumor cells (data not shown). The stable pool generated using the independent ACL shRNA construct pKD-ACL1 (HP 1) was also compared to a vector-transfected pool, as an independent test. The HP 1 cells grew more slowly in vivo than the control-transfected cells inoculated in the contralateral flank of the same mouse (Figure 4C).

To further investigate the underlying mechanism of tumor suppression, we examined tumors resected from nude mice by H&E staining (Figure 4D). Tumors from A549 vector control cells were poorly differentiated and exhibited a disorganized

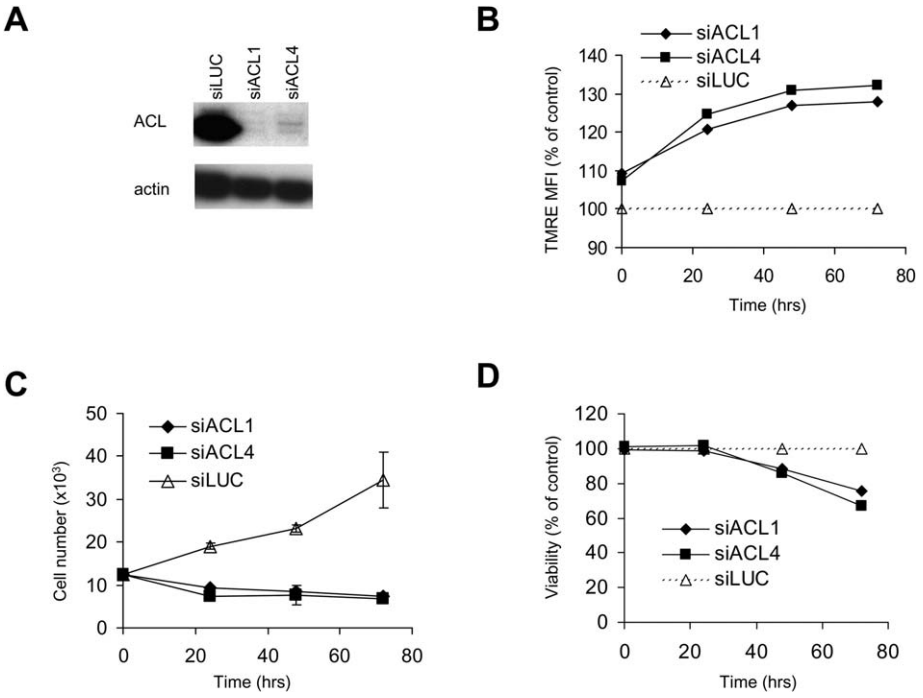

Figure 3. Effects of two independent siRNA hairpins targeting ACL on mitochondrial membrane potential, cell proliferation, and viability of A549 lung cancer cells

A: Efficient knockdown of ACL protein levels by two independent siRNA oligonucleotides in cells transiently transfected with either luciferase (siLUC) or ACL (siACL1, siACL4 corresponding to ACL1, ACL4 siRNA sequences) oligonucleotides. Depicted are curves of mitochondrial membrane potential (MMP) (**B**), cell proliferation (**C**), and viability (**D**) of cells transfected with the indicated siRNA oligonucleotides for two consecutive rounds of transfection. For **B**, MMP was determined by TMRE staining and flow cytometry as described in the Experimental Procedures. The data presented in **B**–**D** correspond to the mean ± standard deviation (SD) from a representative experiment.

cellular architecture (Figure 4D, left panel). In contrast, tumors from clones HP 4-7 and HP 4-8 (Figure 4D, middle panel and data not shown) as well as from the HP 1 pool (Figure 4D, right panel) displayed a more differentiated morphology marked by the presence of glandular structures bearing central lumens. Since mucin production is characteristic of differentiated respiratory epithelium, we examined mucin expression in these tumors by staining with mucicarmine. The tumor nodules recovered from the ACL knockdown cells showed intracytoplasmic and intraluminal mucin staining (Figure 4E, middle and right panels). In contrast, the tumors recovered from the vector control cells, which lacked glandular structures, showed only background staining, consistent with their poorly differentiated phenotype (Figure 4E, left panel). Comparison of vector control versus ACL knockdown tumors with an active caspase-3 antibody found no evidence for the increased presence of apoptotic cells in sections from the latter group (data not shown). Thus, the suppression of tumor growth of A549 cells in vivo upon knockdown of ACL levels is correlated with an increased propensity toward epithelial cell differentiation.

Stable knockdown of endogenous ACL levels by shRNA induces differentiation in the K562 chronic myelogenous leukemia cell line in vitro

The increased degree of differentiation observed in the A549 ACL knockdown tumors in vivo was unexpected. To determine whether the effect was observed in other tumor cell types, we utilized a well-characterized model of in vitro tumor cell differentiation, the human chronic myelogenous leukemia cell line K562, which is dependent on the BCR-ABL fusion protein (Druker et al., 1996). Drugs that inhibit BCR-ABL signaling such as Gleevec (imatinib mesylate) and Hsp90 inhibitors such as radicicol have been promoted as therapeutic agents, based on their ability to induce erythroid differentiation in this tumor model (Druker et al., 1996; Shiotsu et al., 2000). We used an RNAi approach to stably knock down endogenous ACL levels in K562 cells and evaluate downstream effects on cellular differentiation. We generated clones with efficient ACL knockdown by stable transfection of K562 with the pKD-ACL4 shRNA construct (representative clones HP 4-1 and HP 4-2 are shown in Figure 5A). To assess their degree of erythroid differentiation, we analyzed the cells for expression of glycophorin A (CD235a), a surface glycoprotein expressed selectively on erythroid precursors and mature erythrocytes and shown to be induced in K562 cells undergoing erythroid differentiation in response to Gleevec (Kohmura et al., 2004) and radicicol (Shiotsu et al., 2000). Compared to vector control transfected cells, ACL knockdown cells showed an increase in the surface expression of this erythroid cell marker (Figure 5B, left panel), comparable to the induction obtained upon treatment of control cells with the Hsp90 inhibitor radicicol (Figure 5B, right panel). Furthermore, quantitation of hemoglobin-positive cells revealed that approximately 36.7% and 29.3% of cells within the HP 4-1 and HP 4-2 ACL knockdown population, respectively, expressed hemoglobin, compared to 5% of vector control K562 cells (Figure 5C).

Inhibition of ACL activity by the pharmacologic inhibitor SB-204990

As a complementary approach to RNAi, the effects of the ACL chemical inhibitor SB-204990 (Pearce et al., 1998) on cell growth and proliferation were analyzed. In order to evaluate the effects of ACL inhibition by SB-204990 under conditions where both glycolysis and cell proliferation can be regulated, we examined IL-3-dependent cell lines. IL-3 has been shown to directly stimulate glycolysis and cell proliferation in these cell

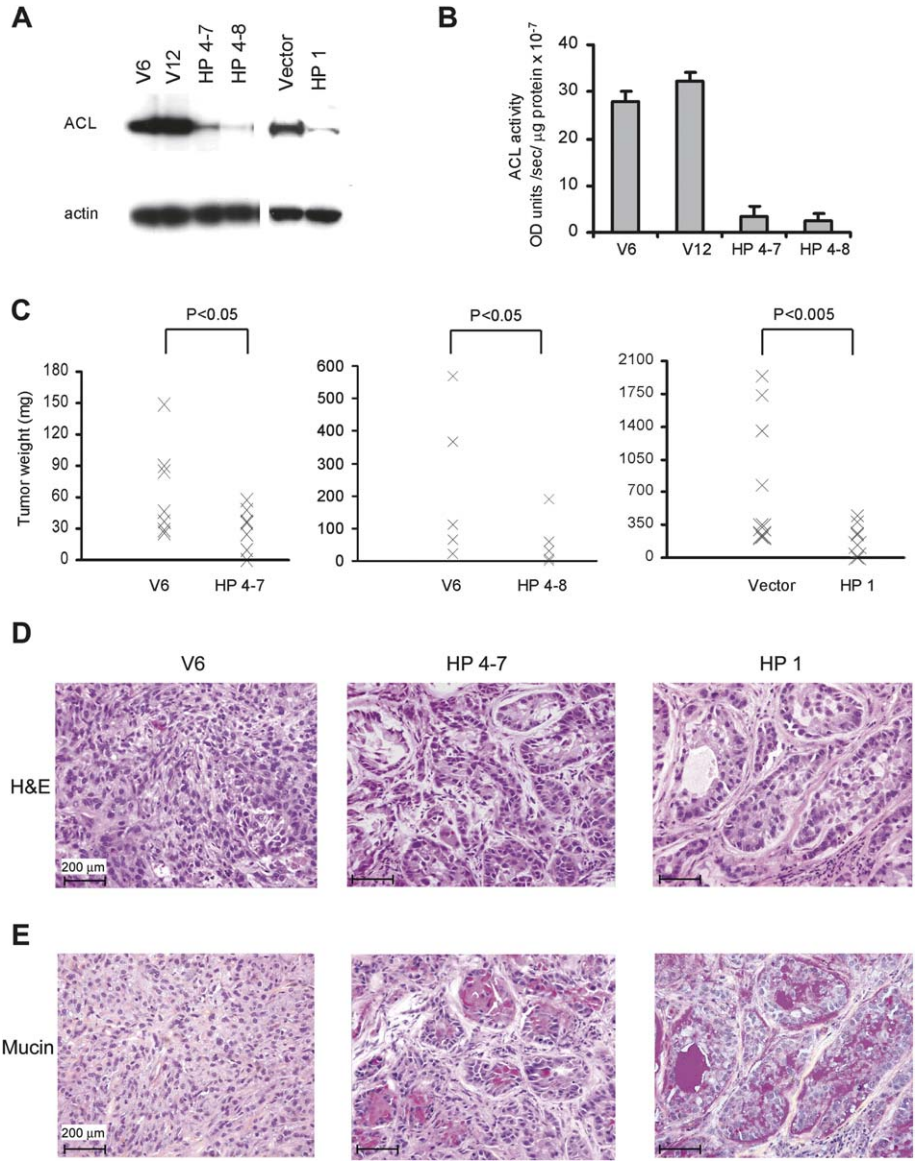

Figure 4. Stable knockdown of ACL levels in A549 cells results in the generation of smaller tumors in vivo displaying features of glandular differentiation

A: Western blot analysis of cellular extracts demonstrates efficient knockdown of ACL levels in A549 cells stably transfected with ACL shRNA constructs. The independent clones V6 and V12 were generated by stable transfection of control pKD vector, while clones HP 4-7 and HP 4-8 were generated using the pKD-ACL4 shRNA plasmid. At right, extracts from pools of cells stably transfected with either empty pKD vector (Vector) or with a different ACL shRNA plasmid [pKD-ACL1(HP 1)] were compared for levels of ACL.

B: ACL activity was measured in protein extracts of either control (V6, V12) or the ACL shRNA stable clones (HP 4-7, HP 4-8) shown above (**A**). Plotted is the mean ± SD of triplicate samples.

C: Charts depicting the weight of subcutaneous tumors formed in nude mice 60 days after injection of either the control (V6, Vector) or the ACL knockdown A549 stable transfectants (HP 4-7 [n = 7], HP 4-8 [n = 5], HP 1 [n = 10]) described above (**A**).

D and E: Glandular differentiation is detected by H&E staining (**D**), and mucin production is detected by mucicarmine staining (**E**) in tumors originating from the ACL knockdown stable transfectants (HP 4-7, HP 1). Original magnification is 200×.

lines (Lum et al., 2005; Plas et al., 2001). A 2 hr preincubation of cells growing in IL-3 with SB-204990 caused a dose-dependent decrease in D-[6-^{14}C]glucose-dependent lipid synthesis (Figure 6A). Synthesis of phospholipids accounted for the bulk of de novo lipogenesis and was thus severely impaired by ACL inhibition (data not shown). In agreement with the RNAi results, ACL inhibition by SB-204990 induced a dose- and time-dependent increase in the MMP of cells proliferating in the presence of IL-3 (Figure 6B and data not shown). These effects were observed in two individual IL-3-dependent cell lines. Furthermore, when IL-3-dependent cells were treated for 24 hr with increasing doses of SB-204990, their proliferation was inhibited, and the cells displayed a dose-dependent G1 cell cycle arrest (Figure 6C). To assay the effects of ACL inhibition on cell growth and cell cycle entry of G1-arrested cells, we initially withdrew growth factor from the IL-3-dependent *Bax*$^{-/-}$*Bak*$^{-/-}$ cells for 5 days and confirmed their G1 arrest (data not shown) and their decrease in cell size (Figure 6D, upper panel) concomitantly with the downregulation of their glycolytic metabolism upon growth factor withdrawal (Lum et al., 2005). Upon readdition of IL-3, the cells are expected to progressively increase in cell size and eventually reenter the cell cycle (Lum et al., 2005). Indeed, vehicle-treated cells were able to increase their cell size and enter the cell cycle 72 hr post-IL-3 addition (Figure 6D and data not shown). In contrast, treatment with increasing doses of SB-204990 resulted in a dose-dependent inhibition of both cell growth and cell cycle entry (Figure 6D and data not shown). In cells treated with the 15 μM SB-204990 dose, cell cycle entry was delayed by 2 additional days, while the higher doses inhibited cell cycle entry almost completely.

In vitro antitumor activity of the chemical ACL inhibitor SB-204990

To test the promise of the ACL inhibitor SB-204990 as a potential cancer therapeutic, three human tumor cell lines from the NIH 60 panel were analyzed for their in vitro sensitivity to ACL

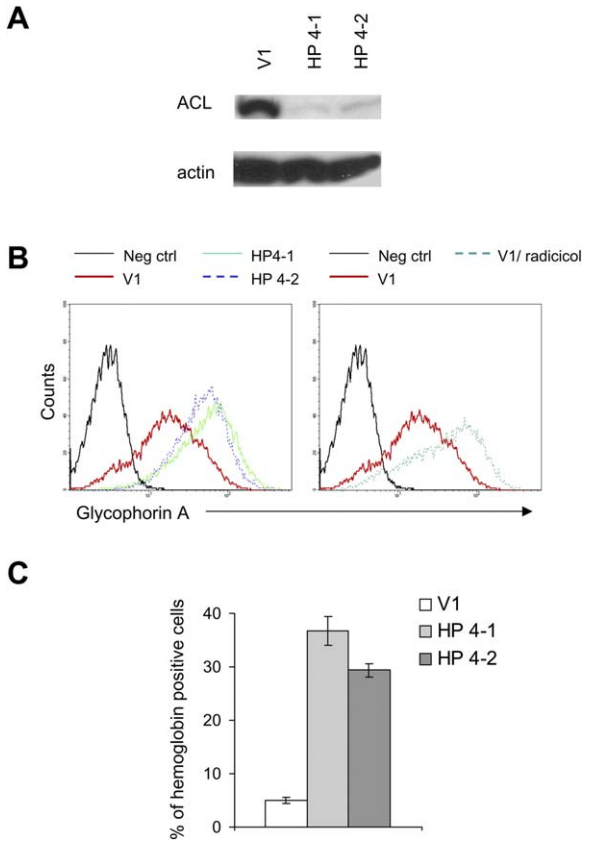

Figure 5. Stable knockdown of ACL levels in the K562 chronic myelogenous leukemia cell line induces erythroid differentiation

A: Western blot analysis demonstrates efficient knockdown of ACL levels in K562 cells stably transfected with ACL shRNA constructs. The V1 clone was generated by stable transfection of control pKD vector, while clones HP 4-1 and HP 4-2 were generated using the pKD-ACL4 shRNA plasmid.

B: Expression levels of the erythroid marker glycophorin A on the surface of control (V1) and ACL knockdown cells (HP 4-1 and HP 4-2) were compared using a mouse FITC-conjugated anti-human glycophorin A antibody. As a negative control (Neg ctrl), cells were incubated with FITC-conjugated control IgG. On the right panel, control K562 cells (V1) were left untreated or were treated with 1.5 μM radicicol for 24 hr prior to analysis, as a positive control for glycophorin A induction.

C: The percentage of hemoglobin-expressing cells in control (V1) and ACL knockdown (HP 4-1 and HP 4-2) cell populations was determined by benzidine staining. Plotted is the mean ± SD of triplicate samples from a representative experiment.

inhibition by SB-204990 and for their ability to form tumors in nude mice. In addition to the A549 cell line that we had previously characterized with RNAi, the cell lines PC3 and SKOV3 were examined. In vitro, all three cell lines displayed a dose- and time-dependent sensitivity to ACL inhibition by SB-204990 (Figure 7A). Measurement of acetyl-CoA following a brief treatment with SB-204990 confirmed that there was a significant and reproducible reduction in total acetyl-CoA levels in treated cells compared to controls (17% reduction; $p < 0.001$; $n = 12$). Interestingly, among the cell lines tested, SKOV3 cells were significantly more resistant to the ACL inhibitor, with a 2-fold higher IC_{50} value (Figure 7A). The differences in sensitivity correlated with the rates of glucose utilization (Figure 7B) and lactate production (Figure 7C) of the cell lines. SKOV3 cells utilize virtually all the glucose they take up, secreting little lactate into the medium. In contrast, A549 and PC3 cells utilize much higher levels of glucose and secrete a large percentage of the glucose carbons they take up into the medium as lactate (Figures 7B and 7C). Consistently with their higher rate of glycolysis (data not shown), A549 and PC3 cells exhibited a 3- to 4-fold higher rate of D-[6-^{14}C]glucose-dependent lipid synthesis than SKOV3 cells (Figure 7D).

To further define the requirements for sensitivity to ACL inhibition in glucose-dependent cells, we utilized a genetic model of paired wild-type and cytochrome c null mouse embryonic cell lines (Mansfield et al., 2005). The latter cells lack a functional mitochondrial respiratory chain and are thus solely dependent on anaerobic glycolysis for their ATP demands. Since these cells cannot oxidize NADH through electron transport, glycolytic pyruvate is preferentially secreted as lactate rather than entering the mitochondrial TCA cycle. As a result, cytochrome c null cells exhibited a 4-fold lower rate of D-[6-^{14}C] glucose-dependent lipid synthesis and a 2.5-fold increase in acetate-to-lipid synthesis in comparison to wild-type cells (see Figure S1A in the Supplemental Data available with this article online). In addition, cytochrome c null cells were significantly more resistant to SB-204990 than their wild-type counterparts (Figure S1B). Thus, cells lacking in the ability to engage in aerobic glycolysis display reduced dependence on glucose-dependent lipid synthesis and ACL activity.

In vivo antitumor activity of the chemical ACL inhibitor SB-204990

To evaluate the antineoplastic activity of SB-204990 in vivo, we utilized xenograft tumor models in nude mice using the three cell lines from the NIH 60 panel described above. In comparison to treatment with vehicle alone, SB-204990 showed significant antineoplastic activity against both A549 and PC3 xenografts (Figure 7E). The effects of the ACL inhibitor in vivo appeared to be cytostatic, as both A549 and PC3 xenografts showed significant inhibition of tumor growth but no tumor regression during the treatment period. Histologic comparison of control- and SB-204990-treated A549 xenografts revealed a more differentiated morphology in the latter group, which was marked by the presence of glandular structures showing intracytoplasmic and intraluminal mucin expression (Figure S2) and similar to what we previously observed upon genetic knockdown of ACL levels in A549 cells (Figure 4E). Analysis of tumor sections for caspase activation to detect apoptotic cells confirmed that the effects of the treatment were predominantly cytostatic, as no significant difference in active caspase-3-positive cells was observed between the ACL-treated and control-treated tumors (Figure S2). No effect of SB-204990 treatment was observed on SKOV3 xenografts in three independent experiments. Mice treated with the SB-204990 drug sustained a significant decrease in their body weight compared to controls. While vehicle-treated mice displayed a 2.1% ± 0.6% weight gain upon completion of treatment, their SB-204990-treated counterparts sustained a 6.8% ± 1.2% weight loss. Similar declines in body weight have been reported previously for ACL inhibitors (Pearce et al., 1998; Shara et al., 2003).

To extend the analysis of the in vivo efficacy of SB-204990, two independent primary pancreatic ductal cell lines were examined (Figure 8). These cell lines were derived from mice expressing endogenous oncogenic *K-ras^{G12D}* (Hingorani et al., 2003) in a p53 wild-type (Figure 8A) or p53 point mutant back-

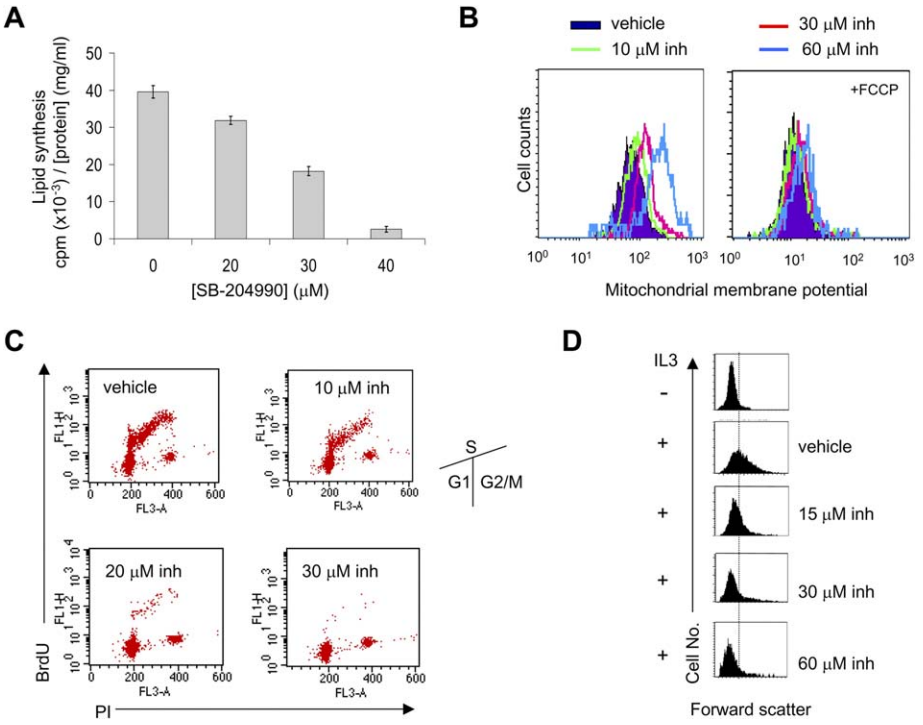

Figure 6. Effects of the chemical ACL inhibitor SB-204990 on lipid synthesis, mitochondrial membrane potential, cell cycle progression, and cell growth

A: Bcl-x_L FL5.12 cells (Plas et al., 2001) were incubated for 2 hr with the indicated doses of SB-204990 or vehicle followed by an additional 2 hr incubation with D-[6-^{14}C]glucose as the radioactive precursor for lipid synthesis. Plotted is the mean ± SEM of triplicate samples from a representative experiment.

B: Bcl-x_L FL5.12 cells were incubated for 2 hr with the indicated doses of SB-204990 (inh) or vehicle followed by staining with TMRE in the presence or absence of the uncoupler FCCP for the flow cytometric determination of mitochondrial membrane potential.

C: IL-3-dependent hematopoietic *Bax*$^{-/-}$*Bak*$^{-/-}$ cells (Lum et al., 2005) were pulse labeled with 10 μM BrdU after a prior 24 hr incubation with the indicated doses of SB-204990 (inh) or vehicle and analyzed for BrdU incorporation and DNA content (PI) to determine cell cycle progression.

D: The *Bax*$^{-/-}$*Bak*$^{-/-}$ IL-3-dependent cells were withdrawn from IL-3 for 5 days, at which point IL-3 was readded to the media in the presence of vehicle or the indicated doses of SB-204990 (inh) and incubated for 72 hr further. Cells were stained with Hoechst 33342 and PI to identify live G1-gated cells. Histograms shown represent the forward scatter of live G1-gated cells as an indicator of cell size.

ground (Figure 8B) (Hingorani et al., 2005) and manifesting preinvasive or invasive pancreatic ductal adenocarcinoma, respectively. Both cell lines have undergone limited passage in vitro compared to the well-established human tumor lines analyzed above (Figure 7). These tumors were chosen because the SB-204990-sensitive A549 cell line also harbors an activating *K-ras* mutation (Mitchell et al., 1995), and Ras has previously been shown to induce tumor cell metabolic conversion to aerobic glycolysis (Blum et al., 2005). Treatment with SB-204990 as described above resulted in significant growth inhibition against xenografts from both cell lines (Figure 8).

Discussion

In this report, we demonstrate that ACL, a key enzyme integrating glucose and lipid metabolism, contributes to de novo glucose-dependent lipid synthesis by tumor cells. Furthermore, genetic and pharmacologic downregulation of ACL activity in cancer cell lines results in a dose-dependent inhibition of cell proliferation in vitro and tumor growth in vivo. The ability of ACL inhibition to suppress tumor growth correlates with the glycolytic phenotype of the tumor. Cancer cells displaying high rates of glucose metabolism are more severely affected, whereas those displaying a low rate of aerobic glycolysis are largely unaffected. The basis for the different sensitivity profiles of tumor cells to ACL inhibition is consistent with a model in which cells with a higher flux of glycolytic carbons from the cytosol to the mitochondria depend on glucose for lipid synthesis necessary to support their growth to a greater extent than their less glycolytic counterparts. The fact that ACL levels and activity can increase through the same signaling pathways that stimulate glycolytic metabolism and that are often deregulated in glycolytic tumors (the PI3K/Akt pathway) (Berwick et al., 2002; Board and Newsholme, 1996) suggests that this upregulation of ACL contributes significantly to the growth advantage and proliferation rate of tumors displaying aerobic glycolysis.

A predicted consequence of ACL downregulation is the impairment of glucose-dependent lipid synthesis, which we have documented by both genetic and pharmacologic means. However, the failure of ACL downregulation to inhibit the growth of tumors that do not display high levels of aerobic glycolysis suggests that there are alternative salvage lipogenic pathways that tumor cells can use to produce acetyl-CoA independently of ACL. Cytosolic acetyl-CoA can also be generated from acetate via cytoplasmic ACAS2 (Sone et al., 2002). ACAS2 activity is present in the cell lines that we analyzed and leads to the incorporation of [1-^{14}C]acetate into lipids in a manner that is not affected by ACL inhibition. In cells displaying low rates of aerobic glycolysis, this pathway may compensate for the low rates of glucose-dependent lipid synthesis, as we observed in cytochrome c null cells. However, acetate is not an abundant metabolite, and its conversion to acetyl-CoA is an energy-dependent process, while the production of acetyl-CoA from glucose is energy producing (see Figure 1).

Our work suggests that the rate of acetyl-CoA generation by salvage pathways independent of ACL can be sufficient to maintain macromolecular synthesis in quantities that support transformation. Thus, ACL inhibitors, like statins, farnesyl transferase inhibitors, and FAS inhibitors are unlikely to be effective therapeutics for all cancers. However, our data predict that tumors displaying a high rate of aerobic glycolysis are likely to be more dependent on ACL for the generation of cytosolic acetyl-CoA. For these tumors, ACL inhibition provides a potential advantage over strategies targeting other lipogenic enzymes

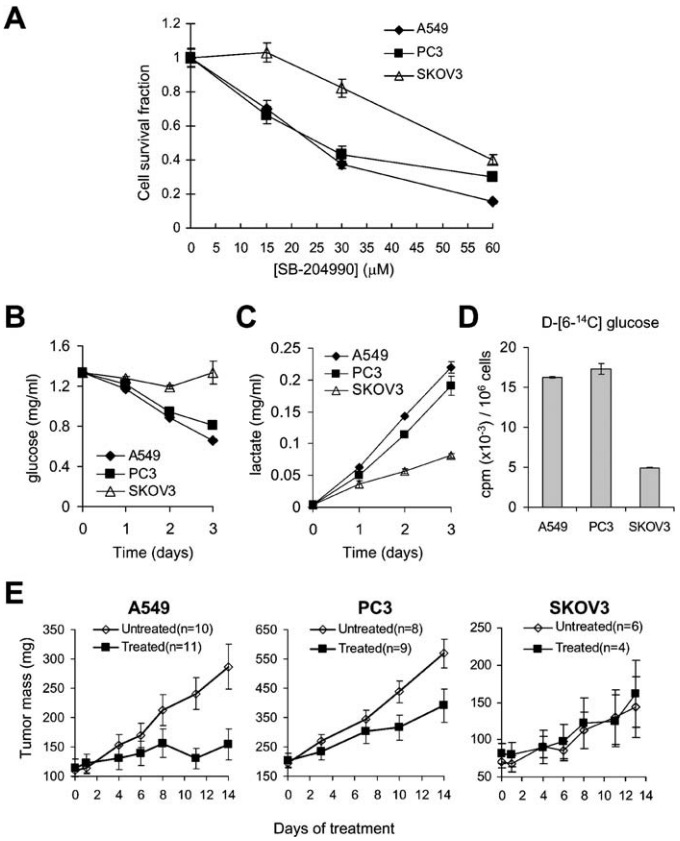

Figure 7. The sensitivity profile of human cancer cell lines to ACL inhibition by SB-204990 in vitro and in vivo correlates with their dependence on glycolytic metabolism

A: The in vitro sensitivity of three human cancer cell lines to SB-204990 was determined as described in the Experimental Procedures, after a 3 day treatment. Plotted is the mean ± SD of triplicate samples from a representative experiment. IC_{50} values for A549, PC3, and SKOV3 were 24 μM, 26 μM, and 53 μM, respectively.

B and C: Tumor cell lines were plated at equal densities and fed fresh media plus 1% FCS at time 0. The concentrations of glucose (**B**) and lactate (**C**) in the media were determined over a 3 day period as described in the Experimental Procedures. Data points represent the mean ± SD of triplicate samples.

D: Tumor cell lines were preincubated in media plus 1% FCS for 24 hr, and the level of their glucose-dependent lipid synthesis was determined as described in the Experimental Procedures. Data points represent the mean ± SD of triplicate samples.

E: Tumors were established in athymic nude female mice by subcutaneous injection of the indicated cancer cell lines. Cohorts of mice with comparable rates of tumor growth were divided randomly into untreated and SB-204990-treated groups (day 0) and treated with vehicle or SB-204990, as described in the Experimental Procedures. Graphed is the mean tumor mass ± SEM from an experiment that is representative of three independent experiments.

because ACL is located upstream of the other lipogenic enzymes. Thus, ACL inhibition can affect the cholesterol, isoprenoid, and fatty acid synthesis pathways in combination (Figure 1). In addition, ACL inhibition affects mitochondrial homeostasis and membrane potential, presumably through the increased availability of mitochondrial citrate for full oxidation and NADH production in the TCA cycle, as previously observed upon ACL inhibition by hydroxycitrate (Board and Newsholme, 1996). Owing to its novel mechanism of action, it should be beneficial to inhibit ACL in combination with other agents used to treat patients with advanced malignancies, such as agents that block oncogenic receptor signaling (Tibes et al., 2005). Since many of these oncogenic signaling cascades activate the PI3K/Akt pathway, which regulates both glucose and lipid metabolism (Elstrom et al., 2004) as well as ACL levels and activity (Berwick et al., 2002), ACL inhibition in combination with tyrosine kinase or PI3K/Akt inhibitors may act to further abrogate the metabolic effects downstream of PI3K/Akt activation.

Another striking phenotype that we observed upon both genetic and pharmacologic ACL inhibition, namely the inhibition of tumor growth and induction of differentiation, has previously been observed by other manipulations that suppress glycolysis in tumor cells, such as inhibition of the insulin-like growth factor I receptor (IGF-IR) by stable expression of a dominant-negative IGF-IR in A549 cells (Jiang et al., 1999) or inhibition of BCR-ABL signaling by treatment with Gleevec in K562 cells (Boren et al., 2001). Furthermore, previous work has shown the induction of differentiation in the HT29 colon adenocarcinoma tumor cell line model, upon incubation of cells with butyrate, which can act as an alternative substrate for mitochondrial oxidation and lipogenesis, in place of glucose (Boren et al., 2003). A decrease in aerobic glycolysis and glucose-dependent lipid synthesis was observed in butyrate-treated cells. Together, these results suggest that aerobic glycolysis may contribute to the suppression of tumor cell differentiation by stimulating cytosolic acetyl-CoA production and lipid synthesis through ACL. Upon interruption of its high glucose-to-lipid flux, factors in the in vivo tumor microenvironment may allow a tumor cell to initiate adaptive responses, such as differentiation, in order to maintain its survival. It is tempting to speculate that certain glycolytically derived metabolic intermediates may serve as signals orchestrating these events. One of these intermediates is glycolytically derived citrate. Disrupting citrate transport to the cytosol may be another potential strategy for targeting glycolytically converted tumors.

In conclusion, the conversion of tumors to a highly glucose-dependent metabolism, as measured by FDG-PET imaging, identifies a group of advanced malignancies, for which few therapeutic options currently exist. Here, we demonstrate that this conversion to a glucose-dependent metabolism (aerobic glycolysis) significantly enhances the rate at which tumors grow and that at least part of this increased growth comes from increased, glucose-dependent production of cytosolic acetyl-CoA by ACL. ACL inhibition, either by being cytostatic for cells exhibiting glucose-dependent growth or by inducing differentiation, provides a novel mechanism to suppress cancer progression. As an antineoplastic strategy, ACL inhibition would be relatively tumor-selective and spare normal tissues, since vegetative and nonglycolytic cells are significantly less dependent on ACL activity.

Experimental procedures

Cell culture

Cell culture reagents were purchased from Invitrogen (Carlsbad, CA), unless otherwise indicated. IL-3-dependent cell lines were grown in the presence or absence of IL-3 as previously described (Plas et al., 2001; Lum et al., 2005). The human cancer cell lines A549, PC3, SKOV3, and K562 were obtained from the ATCC (Manassas, VA) and grown in medium supplemented with 10% heat-inactivated fetal calf serum (Gemini), 10 mM HEPES, 100 U/ml penicillin, 100 μg/ml streptomycin. The cytochrome c null and

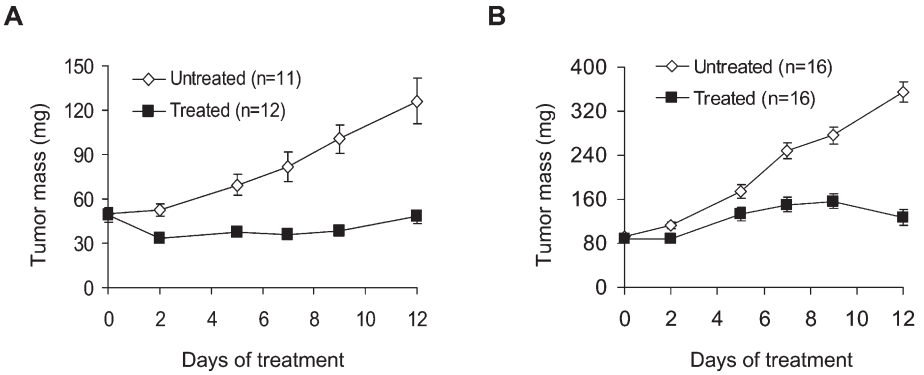

Figure 8. Inhibition of tumor growth by intraperitoneal administration of SB-204990 in nude mice carrying xenografts of mouse pancreatic ductal cell lines bearing oncogenic *K-ras*^{G12D} alleles

Tumors were established in athymic nude female mice by subcutaneous injection of the indicated cell lines. Cohorts of mice with comparable rates of tumor growth were divided randomly into untreated and SB-204990-treated groups (day 0) and treated by i.p. injection of SB-204990 at a dose of 350 μmol/kg/day (135 mg/kg/day) once daily for 12 days. Graphed is the mean tumor mass ± SEM.

wild-type mouse embryonic cell lines were cultured as previously described (Mansfield et al., 2005).

Flow cytometry

For cell cycle analysis, triplicate samples of cells were pulsed for 90 min with 10 μM BrdU (Sigma) and were then fixed, stained with an anti-BrdU mAb (PharMingen) and propidium iodide (PI), and analyzed by flow cytometry using an LSR flow cytometer (BD Biosciences). Cell viability was determined by the exclusion of 10 μg/ml DAPI (Molecular Probes) as determined by flow cytometry. To examine MMP, cells were stained in triplicate with 20 nM tetramethyl rhodamine ethyl ester (TMRE; Molecular Probes) and 10 μg/ml DAPI (Molecular Probes) for 30 min at 37°C in the presence or absence of the mitochondrial uncoupler FCCP (50 μM; Sigma).

Western blotting

Equivalent amounts of total cell protein were loaded onto 4%–12% Bis-Tris gels (Invitrogen), as previously described (Lum et al., 2005). Proteins were transferred to a PVDF membrane, membranes were blocked with BLOTTO (5% nonfat dry milk and 0.1% Tween 20 in PBS) and incubated with a rabbit antiserum generated against the ACL peptide IGHYLDQKRLKQGLYRH (1:1000) or with a mouse anti-actin antibody (1:10,000) (Sigma A5441) at 4°C overnight. Membranes were washed in PBS plus 0.1% Tween 20 and probed with anti-rabbit or anti-mouse HRP-conjugated secondary antibody (both at 1:10,000 dilution), and proteins were detected using the ECL Plus chemiluminescence detection reagent (Amersham Biosciences).

siRNA, shRNA, and transfections

siRNA oligonucleotides targeting ACL and control siRNA-targeting luciferase were obtained from Invitrogen. The ACL1 siRNA sequence is 5′-GCCA GAACUUGGUAGUCAATT-3′. The ACL4 siRNA sequence is 5′-GGCAUGUC CAACGAGCUCAATT-3′. The luciferase siRNA sequence is 5′-CGUACGC GGAAUACUUCGATT-3′. Transfections were performed using Lipofectamine 2000 (Invitrogen) according to the manufacturer's instructions. Briefly, 4 μl of a 20 μM siRNA solution and 2 μl of Lipofectamine 2000 were incubated in 200 μl of serum-free Optimem media (Invitrogen) for 20 min and overlaid onto cells cultured in 1 ml of DMEM, 10% FCS without pen/strep in a 12-well plate. The pKD shRNA constructs used to express short hairpins for RNAi were derived as previously described (Edinger et al., 2003). The ACL4 shRNA sequence (sense) is 5′-GGCATGTCCAACGAGCTCAA-3′. The ACL1 shRNA is 5′-GCCTCTTCAATTTCTACGAGGACTT-3′. Stable clones were selected by puromycin resistance followed by limiting dilution.

Lipid synthesis

Samples were assayed for lipid synthesis through D-[6-^{14}C]glucose or [1-^{14}C]acetate in triplicate. To begin the assay, 4 μCi/ml D-[6-^{14}C]glucose (72 μM final concentration) or 2 μCi/ml [1-^{14}C]acetate (36 μM final concentration) was added to the cells, and cells were incubated at 37°C for 2 hr. For experiments measuring inhibition of lipid synthesis by the ACL inhibitor SB-204990, cells were preincubated with the drug (60 μM) for 2 hr prior to the addition of the radioactive lipid precursors. For adherent cells grown on a 12-well plate, lipids were extracted by the addition of 500 μl of a hexane:isopropanol solution (3:2 ratio). Wells were washed with an additional 500 μl of hexane:isopropanol solution, and extracts were combined and dried under N_2, resuspended in 50 μl of chloroform, and counted in ScintiVerse (Fisher) on a Beckman LS 6500 scintillation counter. Protein concentration was determined by a Lowry protein assay. For suspension cells, cellular lipids were extracted by a modification of the Bligh-Dyer protocol (Bligh and Dyer, 1959).

ACL activity and acetyl-CoA assays

ACL activity was measured via the malate dehydrogenase-coupled method (Srere, 1959). The change in absorbance in the absence of exogenous ATP was subtracted from that in the presence of ATP, and the difference was normalized to the total protein concentration in order to determine the specific ACL activity. Acetyl-CoA was measured by an enzymatic amplification method as previously described (Kato, 1975). Briefly, 3 × 10^6 cells were plated on a 10 cm plate and treated overnight with 60 μM SB-204990 or vehicle. The next day, cells were harvested in PBS, 0.5 mM EDTA, and the pellet was deproteinized in 50 μl 6% perchloric acid and neutralized with 27.2 μl 2 M $KHCO_3$. Twenty microliters of cleared supernatants were incubated at 30°C × 10 min with 5 μl 0.1 mM NEM in 0.5 M Tris (pH 7.4) buffer for CoASH elimination. Five microliter aliquots were then added to a reaction mixture containing 100 mM Tris (pH 7.4), 10 mM NH_4CL, 0.02% w/v BSA, 1.2 mM oxaloacetate, 1.9 mM acetylphosphate, 36 U phosphotransacetylase, 6 U citrate synthase, and 4 μM glutathione and incubated ×1 hr at 30°C. Samples were boiled ×5 min, and 50 μl of supernatants were used for the indicator reaction as previously described (Dagley, 1965).

Glucose and lactate measurements

Tumor cell lines were plated at a concentration of 100,000 cells/ml in RPMI 10% FCS. The following day, medium was replaced with RPMI 1% FCS, and cells were incubated for 3 additional days. Medium samples were collected each day and stored at –20°C until the time of the assay. Glucose and lactate were measured using colorimetric kits according to the manufacturer's instructions (CMA/Microdialysis).

Erythroid differentiation analysis

Induction of surface expression of the erythroid marker glycophorin A was determined by indirect immunofluorescence and flow cytometry. Cells were stained with a mouse FITC-conjugated anti-glycophorin A antibody (Dako) at 1:100 dilution in medium plus 10% FCS for 30 min at 4°C. As a control, cells were stained with FITC-conjugated IgG. Cells expressing hemoglobin were determined by benzidine staining as previously described (Park et al., 2001). The proportion of blue-stained cells was quantified under light microscopy. A total of 500 cells were counted for each sample in triplicate. Shown is the mean ± SD of a representative experiment.

In vitro drug inhibition assay

Cells were plated in 96-well plates at a density of 3000 cells per well and incubated with RPMI medium supplemented with 1% FCS and the indicated concentrations of vehicle or the ACL inhibitor SB-204990. The drug solution was prepared by mixing equimolar amounts of SB-204990 and

sodium bicarbonate in water to achieve a pH of 7.4. At the indicated times, a sulforhodamine B assay was performed using a kit (Sigma, cat. no. TOX6), according to the manufacturer's instructions.

In vivo antitumor activity of ACL inhibition

Early passage, exponentially growing tumor cell lines in culture were harvested and washed twice with PBS before being resuspended in PBS at a concentration of 50×10^6 cells/ml. Tumors were established in athymic nude female mice (8–10 weeks old; Charles River) by subcutaneous injection of 10×10^6 cells in a 200 μl volume. Unless otherwise indicated, the tumor size was measured weekly, and tumors were excised for weight measurements, histological examination, and mucicarmine staining 60 days after cell injection. For the drug treatment groups, cohorts of mice with comparable size tumors were divided randomly 3–5 weeks following tumor cell injection into two groups: untreated (injected with vehicle alone) and treated (injected with SB-204990) animals. The animals were monitored daily until treatment was complete. Body weight and tumor size were measured every 2–3 days. Tumor growth was recorded by the measurement (with calipers) of two perpendicular diameters of the tumor. Tumor mass (in mg) was calculated by the formula $1/2(a \times b^2)$, where a is the long diameter (in mm) and b is the short diameter (in mm) (Wang et al., 1999). SB-204990 was administrated to treated animals via i.p. injection at a dose of 350 μmol/kg/day (135 mg/kg/day) once daily for 14 days. This dose has previously been shown to produce hypolipidemic effects in rodents (Pearce et al., 1998). All procedures were approved by the Institutional Animal Care and Use Committee of the University of Pennsylvania.

Tumor histology and immunohistochemistry

Tumors were excised, formalin fixed for 24 hr, and embedded in paraffin. Sections were cut at 5 μm and stained with Gill's hematoxylin solution #3 and eosin (both from Fisher Scientific) for H&E or with the mucicarmine staining kit (Sigma) for mucin production. Immunohistochemistry for caspase activation was performed using an active caspase-3 rabbit antibody (R&D Systems AF835) at a 1:1000 antibody dilution on an Autostainer Plus automated staining system (DAKOCytomation), according to the manufacturer's instructions. Slides were counterstained with Gill's hematoxylin solution #3.

Statistical analysis

The masses of tumors, generated in nude mice by injection of either vector or ACL knockdown cells in either flank of each mouse, were compared using the Wilcoxon matched-pairs signed-ranks test for matched pairs of nonparametric observations. Glucose- and acetate-dependent lipid synthesis across siLUC versus siACL-treated cells was compared by the Mann-Whitney test for two unmatched samples. All p values are two sided. Statistical analysis was carried out using the STATA program (STATA v.8, STATA Corporation College Station, TX, 2003).

Supplemental data

The Supplemental Data include two supplemental figures and can be found with this article online at http://www.cancercell.org/cgi/content/full/8/4/311/DC1/.

Acknowledgments

The authors thank Debra Cromley and Daniel Martinez for excellent technical assistance and Jeffrey Billheimer, Jane Glick, and members of the Thompson laboratory for helpful discussions and comments on the manuscript. G.H. is a Damon Runyon Fellow supported by the Damon Runyon Cancer Research Foundation (DRG-#1714-02). This work was supported by grants from the NIH and GlaxoSmith-Kline.

Received: April 11, 2005
Revised: September 9, 2005
Accepted: September 28, 2005
Published: October 17, 2005

References

Baggetto, L.G. (1992). Deviant energetic metabolism of glycolytic cancer cells. Biochimie *74*, 959–974.

Bauer, D.E., Harris, M.H., Plas, D.R., Lum, J.J., Hammerman, P.S., Rathmell, J.C., Riley, J.L., and Thompson, C.B. (2004). Cytokine stimulation of aerobic glycolysis in hematopoietic cells exceeds proliferative demand. FASEB J. *18*, 1303–1305.

Berwick, D.C., Hers, I., Heesom, K.J., Moule, S.K., and Tavare, J.M. (2002). The identification of ATP-citrate lyase as a protein kinase B (Akt) substrate in primary adipocytes. J. Biol. Chem. *277*, 33895–33900.

Bligh, E.G., and Dyer, W.J. (1959). A rapid method of total lipid extraction and purification. Can. J. Biochem. Physiol. *37*, 911–917.

Blum, R., Jacob-Hirsch, J., Amariglio, N., Rechavi, G., and Kloog, Y. (2005). Ras inhibition in glioblastoma down-regulates hypoxia-inducible factor-1α, causing glycolysis shutdown and cell death. Cancer Res. *65*, 999–1006.

Board, M., and Newsholme, E. (1996). Hydroxycitrate causes altered pyruvate metabolism by tumorigenic cells. Biochem. Mol. Biol. Int. *40*, 1047–1056.

Boren, J., Cascante, M., Marin, S., Comin-Anduix, B., Centelles, J.J., Lim, S., Bassilian, S., Ahmed, S., Lee, W.N., and Boros, L.G. (2001). Gleevec (STI571) influences metabolic enzyme activities and glucose carbon flow toward nucleic acid and fatty acid synthesis in myeloid tumor cells. J. Biol. Chem. *276*, 37747–37753.

Boren, J., Lee, W.N., Bassilian, S., Centelles, J.J., Lim, S., Ahmed, S., Boros, L.G., and Cascante, M. (2003). The stable isotope-based dynamic metabolic profile of butyrate-induced HT29 cell differentiation. J. Biol. Chem. *278*, 28395–28402.

Buzzai, M., Bauer, D.E., Jones, R.G., Deberardinis, R.J., Hatzivassiliou, G., Elstrom, R.L., and Thompson, C.B. (2005). The glucose dependence of Akt-transformed cells can be reversed by pharmacologic activation of fatty acid β-oxidation. Oncogene *24*, 4165–4173.

Crabtree, H.G. (1929). Observations on the carbohydrate metabolism of tumours. Biochem. J. *23*, 536–545.

Dagley, S. (1965). Citrate, UV spectrophotometric determination. In Methods of Enzymatic Analysis, H.W. Bergmeyer, ed. (New York: Academic Press), pp. 1562–1565.

Dang, C.V., and Semenza, G.L. (1999). Oncogenic alterations of metabolism. Trends Biochem. Sci. *24*, 68–72.

Detterbeck, F.C., Vansteenkiste, J.F., Morris, D.E., Dooms, C.A., Khandani, A.H., and Socinski, M.A. (2004). Seeking a home for a PET, part 3: Emerging applications of positron emission tomography imaging in the management of patients with lung cancer. Chest *126*, 1656–1666.

Druker, B.J., Tamura, S., Buchdunger, E., Ohno, S., Segal, G.M., Fanning, S., Zimmermann, J., and Lydon, N.B. (1996). Effects of a selective inhibitor of the Abl tyrosine kinase on the growth of Bcr-Abl positive cells. Nat. Med. *2*, 561–566.

Edinger, A.L., Cinalli, R.M., and Thompson, C.B. (2003). Rab7 prevents growth factor-independent survival by inhibiting cell-autonomous nutrient transporter expression. Dev. Cell *5*, 571–582.

Elstrom, R.L., Bauer, D.E., Buzzai, M., Karnauskas, R., Harris, M.H., Plas, D.R., Zhuang, H., Cinalli, R.M., Alavi, A., Rudin, C.M., and Thompson, C.B. (2004). Akt stimulates aerobic glycolysis in cancer cells. Cancer Res. *64*, 3892–3899.

Gambhir, S.S. (2002). Molecular imaging of cancer with positron emission tomography. Nat. Rev. Cancer *2*, 683–693.

Hingorani, S.R., Petricoin, E.F., Maitra, A., Rajapakse, V., King, C., Jacobetz, M.A., Ross, S., Conrads, T.P., Veenstra, T.D., Hitt, B.A., et al. (2003). Preinvasive and invasive ductal pancreatic cancer and its early detection in the mouse. Cancer Cell *4*, 437–450.

Hingorani, S.R., Wang, L., Multani, A.S., Combs, C., Deramaudt, T.B., Hruban, R.H., Rustgi, A.K., Chang, S., and Tuveson, D.A. (2005). Trp53R172H and KrasG12D cooperate to promote chromosomal instability and widely metastatic pancreatic ductal adenocarcinoma in mice. Cancer Cell *7*, 469–483.

Jackowski, S., Wang, J., and Baburina, I. (2000). Activity of the phosphatidylcholine biosynthetic pathway modulates the distribution of fatty

acids into glycerolipids in proliferating cells. Biochim. Biophys. Acta *1483*, 301–315.

Jiang, Y., Rom, W.N., Yie, T.A., Chi, C.X., and Tchou-Wong, K.M. (1999). Induction of tumor suppression and glandular differentiation of A549 lung carcinoma cells by dominant-negative IGF-I receptor. Oncogene *18*, 6071–6077.

Kaplan, R.S., Mayor, J.A., and Wood, D.O. (1993). The mitochondrial tricarboxylate transport protein. cDNA cloning, primary structure, and comparison with other mitochondrial transport proteins. J. Biol. Chem. *268*, 13682–13690.

Kato, T. (1975). CoA cycling: an enzymatic amplification method for determination of CoASH and acetyl CoA. Anal. Biochem. *66*, 372–392.

Katz, N.R., and Giffhorn, S. (1983). Glucose- and insulin-dependent induction of ATP citrate lyase in primary cultures of rat hepatocytes. Biochem. J. *212*, 65–71.

Kohmura, K., Miyakawa, Y., Kawai, Y., Ikeda, Y., and Kizaki, M. (2004). Different roles of p38 MAPK and ERK in STI571-induced multi-lineage differentiation of K562 cells. J. Cell. Physiol. *198*, 370–376.

Kuhajda, F.P. (2000). Fatty-acid synthase and human cancer: new perspectives on its role in tumor biology. Nutrition *16*, 202–208.

Lum, J.J., Bauer, D.E., Kong, M., Harris, M.H., Li, C., Lindsten, T., and Thompson, C.B. (2005). Growth factor regulation of autophagy and cell survival in the absence of apoptosis. Cell *120*, 237–248.

Mansfield, K.D., Guzy, R.D., Pan, Y., Young, R.M., Cash, T.P., Schumacker, P.T., and Simon, M.C. (2005). Mitochondrial dysfunction resulting from loss of cytochrome c impairs cellular oxygen sensing and hypoxic HIF-α activation. Cell Metab. *1*, 393–399.

Medes, G., Thomas, A., and Weinhouse, S. (1953). Metabolism of neoplastic tissue. IV. A study of lipid synthesis in neoplastic tissue slices in vitro. Cancer Res. *13*, 27–29.

Mitchell, C.E., Belinsky, S.A., and Lechner, J.F. (1995). Detection and quantitation of mutant K-ras codon 12 restriction fragments by capillary electrophoresis. Anal. Biochem. *224*, 148–153.

Nakashima, R.A., Paggi, M.G., and Pedersen, P.L. (1984). Contributions of glycolysis and oxidative phosphorylation to adenosine 5′-triphosphate production in AS-30D hepatoma cells. Cancer Res. *44*, 5702–5706.

Ookhtens, M., Kannan, R., Lyon, I., and Baker, N. (1984). Liver and adipose tissue contributions to newly formed fatty acids in an ascites tumor. Am. J. Physiol. *247*, R146–R153.

Park, J.I., Choi, H.S., Jeong, J.S., Han, J.Y., and Kim, I.H. (2001). Involvement of p38 kinase in hydroxyurea-induced differentiation of K562 cells. Cell Growth Differ. *12*, 481–486.

Pearce, N.J., Yates, J.W., Berkhout, T.A., Jackson, B., Tew, D., Boyd, H., Camilleri, P., Sweeney, P., Gribble, A.D., Shaw, A., and Groot, P.H. (1998). The role of ATP citrate-lyase in the metabolic regulation of plasma lipids. Hypolipidaemic effects of SB-204990, a lactone prodrug of the potent ATP citrate-lyase inhibitor SB-201076. Biochem. J. *334*, 113–119.

Plas, D.R., Talapatra, S., Edinger, A.L., Rathmell, J.C., and Thompson, C.B. (2001). Akt and Bcl-xL promote growth factor-independent survival through distinct effects on mitochondrial physiology. J. Biol. Chem. *276*, 12041–12048.

Sabine, J.R., Abraham, S., and Chaikoff, I.L. (1967). Control of lipid metabolism in hepatomas: insensitivity of rate of fatty acid and cholesterol synthesis by mouse hepatoma BW7756 to fasting and to feedback control. Cancer Res. *27*, 793–799.

Shara, M., Ohia, S.E., Yasmin, T., Zardetto-Smith, A., Kincaid, A., Bagchi, M., Chatterjee, A., Bagchi, D., and Stohs, S.J. (2003). Dose- and time-dependent effects of a novel (–)-hydroxycitric acid extract on body weight, hepatic and testicular lipid peroxidation, DNA fragmentation and histopathological data over a period of 90 days. Mol. Cell. Biochem. *254*, 339–346.

Shiotsu, Y., Neckers, L.M., Wortman, I., An, W.G., Schulte, T.W., Soga, S., Murakata, C., Tamaoki, T., and Akinaga, S. (2000). Novel oxime derivatives of radicicol induce erythroid differentiation associated with preferential G(1) phase accumulation against chronic myelogenous leukemia cells through destabilization of Bcr-Abl with Hsp90 complex. Blood *96*, 2284–2291.

Sone, H., Shimano, H., Sakakura, Y., Inoue, N., Amemiya-Kudo, M., Yahagi, N., Osawa, M., Suzuki, H., Yokoo, T., Takahashi, A., et al. (2002). Acetyl-coenzyme A synthetase is a lipogenic enzyme controlled by SREBP-1 and energy status. Am. J. Physiol. Endocrinol. Metab. *282*, E222–E230.

Srere, P. (1959). The citrate cleavage enzyme. I. Distribution and purification. J. Biol. Chem. *234*, 2544–2547.

Szutowicz, A., Kwiatkowski, J., and Angielski, S. (1979). Lipogenetic and glycolytic enzyme activities in carcinoma and nonmalignant diseases of the human breast. Br. J. Cancer *39*, 681–687.

Tibes, R., Trent, J., and Kurzrock, R. (2005). Tyrosine kinase inhibitors and the dawn of molecular cancer therapeutics. Annu. Rev. Pharmacol. Toxicol. *45*, 357–384.

Towle, H.C., Kaytor, E.N., and Shih, H.M. (1997). Regulation of the expression of lipogenic enzyme genes by carbohydrate. Annu. Rev. Nutr. *17*, 405–433.

Turyn, J., Schlichtholz, B., Dettlaff-Pokora, A., Presler, M., Goyke, E., Matuszewski, M., Kmiec, Z., Krajka, K., and Swierczynski, J. (2003). Increased activity of glycerol 3-phosphate dehydrogenase and other lipogenic enzymes in human bladder cancer. Horm. Metab. Res. *35*, 565–569.

Wang, H., Cai, Q., Zeng, X., Yu, D., Agrawal, S., and Zhang, R. (1999). Antitumor activity and pharmacokinetics of a mixed-backbone antisense oligonucleotide targeted to the RIα subunit of protein kinase A after oral administration. Proc. Natl. Acad. Sci. USA *96*, 13989–13994.

Warburg, O. (1956). On the origin of cancer cells. Science *123*, 309–314.

Zambell, K.L., Fitch, M.D., and Fleming, S.E. (2003). Acetate and butyrate are the major substrates for de novo lipogenesis in rat colonic epithelial cells. J. Nutr. *133*, 3509–3515.